Available online at www.sciencedirect.com
SCIENCE DIRECT
Icarus 180 (2006) 113–123
ICARUS
www.elsevier.com/locate/icarus

Interaction of moist convection with zonal jets on Jupiter and Saturn

Liming Li [a,*], Andrew P. Ingersoll [a], Xianglei Huang [b]

[a] *Division of Geological and Planetary Sciences, MS 150-21, California Institute of Technology, Pasadena, CA 91125, USA*
[b] *Program in Atmospheric and Oceanic Sciences, Princeton University, Princeton, NJ 08544-0710, USA*

Received 4 March 2005; revised 22 July 2005

Available online 9 November 2005

Abstract

Observations suggest that moist convection plays an important role in the large-scale dynamics of Jupiter's and Saturn's atmospheres. Here we use a reduced-gravity quasigeostrophic model, with a parameterization of moist convection that is based on observations, to study the interaction between moist convection and zonal jets on Jupiter and Saturn. Stable jets with approximately the same width and strength as observations are generated in the model. The observed zonal jets violate the barotropic stability criterion but the modeled jets do so only if the flow in the deep underlying layer is westward. The model results suggest that a length scale and a velocity scale associated with moist convection control the width and strength of the jets. The length scale and velocity scale offer a possible explanation of why the jets of Saturn are stronger and wider than those of Jupiter.

Keywords: Jupiter, atmosphere; Saturn, atmosphere; Atmospheres, dynamics

1. Introduction

Multiple zonal jets in each hemisphere of Jupiter have been constant (Garcia-Melendo and Sanchez-Lavega, 2001; Porco et al., 2003) in location and intensity since Voyager times even though some westward jets violate the barotropic stability criterion (Ingersoll et al., 1981; Limaye, 1986; Li et al., 2004). The jets outside the equatorial regions on Saturn are constant with time. HST observations (Sanchez-Lavega et al., 2003) and recent Cassini observations (Porco et al., 2005) suggest that the equatorial jets may be constant in time as well, and that only the altitude of the visible clouds has changed.

Rhines (1975) first demonstrated that zonal jets emerge from decaying turbulence, during a process known as an inverse energy cascade. Williams (1978) first applied these ideas to Jupiter. Voyager observations (Beebe et al., 1980; Ingersoll et al., 1981, 1984) showed that the inverse cascade of energy plays an important role in the atmospheres of Jupiter and Saturn. Many two-dimensional turbulence models have addressed the large-scale dynamics of the giant planets in this way. The forced-dissipative turbulence models (Huang and Robinson, 1998; Marcus et al., 2000) use either a random Markov process or positive and negative sources of vorticity at a prescribed scale. The decaying turbulence models (Cho and Polvani, 1996) drive their simulation by an initial eddy field. One model (Panetta, 1993) is forced by a prescribed vertical shear of the zonal wind, which generates the turbulence. In all these models, the forces are prescribed, and are not affected by any feedback from the flow that develops. All models succeed in producing jets from turbulence, but the jets are not as intense as the observed jets in Jupiter and Saturn: In these models, the largest value of the curvature of zonal jets U_{yy} is never larger than 0.3β. Here U is the mean zonal wind (positive eastward), y is the northward coordinate, and β is the planetary vorticity gradient. On Jupiter the largest values of U_{yy} are of order 2β (Ingersoll et al., 1981; Limaye, 1986; Li et al., 2004).

Models of the thermochemical structure suggest that moist convection (MC) exists in the atmospheres of Jupiter and Saturn (Lewis, 1969; Weidenschilling and Lewis, 1973). Observations from Voyager, ground-based telescopes, and HST show that a rich meteorological activity including convective storms exists there as well (Hunt et al., 1982; Carlson et al., 1992;

* Corresponding author.
E-mail address: liming@gps.caltech.edu (L. Li).

0019-1035/$ – see front matter
doi:10.1016/j.icarus.2005.08.016

Sanchez-Lavega et al., 1999). The Galileo orbiter and Cassini flyby revealed important new information about MC in Jupiter's atmosphere. The relative humidity of water varies from 10^{-2} to 1.0 at the 260 K level (Roos-Serote et al., 2000). Lightning, which is a good indicator of MC, is associated with small ($<$1000 km), distinct, widely-separated cloud features that appear suddenly in the cyclonic regions (Little et al., 1999; Porco et al., 2003) and extend to great height (Banfield et al., 1998). The MC features are anticyclones (Gierasch et al., 2000; Li et al., 2004), although they appear in cyclonic shear zones. Generally they are either swallowed by the larger anticyclonic ovals like the Great Red Spot (GRS) or pulled apart by the shear of the zonal jets (Li et al., 2004).

One interpretation (Gierasch et al., 2000; Ingersoll et al., 2000) of these observations is that MC is providing energy to the large-scale flow structures in Jupiter's atmosphere. Our model is based on the following concepts: The weather layer, which is the region between the base of the water cloud at $\sim$6 bars and the level of emission to space at $\sim$0.4 bars, rests hydrostatically on a much deeper lower layer. The interface is stable, so the potential temperature of the weather layer is greater than that of the lower layer. Heat from the planet's interior converts lower layer parcels into parcels whose potential temperature is equal to that of the weather layer. These parcels rise into the weather layer during a MC event. Steady radiative cooling converts weather layer fluid back into low-entropy fluid of the lower layer, so there is a net long-term balance. The MC events are triggered whenever the weather layer thickness falls below a certain threshold, which means that the MC events appear in the cyclonic regions, as observed. The injection of mass into the weather layer generates mesoscale anticyclonic (negative) vorticity (Little et al., 1999; Gierasch et al., 2000; Li et al., 2004), and the steady radiative cooling generates large-scale cyclonic (positive) vorticity. During the adjustment between the mesoscale forcing from MC and the large-scale forcing from radiation, the mechanical energy of mesoscale vortices is transferred to large-scale structures, i.e., the GRS and zonal jets, by merging with them in an inverse energy cascade (Beebe et al., 1980; Ingersoll et al., 1981, 1984).

There have been several numerical simulations of MC on Jupiter and Saturn (Stoker, 1986; Yair et al., 1992, 1995; Hueso et al., 2002; Hueso and Sanchez-Lavega, 2001, 2004). However, the numerical simulation of the interactions between MC and the large-scale dynamics is a relatively new field partly due to the large difference in scale between the mesoscale processes and the large-scale dynamics. In this paper, we parameterize MC using the available observations, and we study its role in maintaining the large-scale flow structures in the atmospheres of Jupiter and Saturn. We take the motions below the weather layer into account in order to get intense westward jets with curvature larger than β. These ideas are tested by a reduced-gravity quasigeostrophic (QG) model.

The assumptions of the QG model do not hold near the equator, so we cannot study the equatorial jets, which are strong and westerly on Jupiter and Saturn. A shallow water model (Cho and Polvani, 1996) generates strong easterly jets at the equator. Deep convection extending through the planet from north to south (Busse, 1976) makes westerly equatorial jets possible in theory. Numerical models of deep convection (Sun et al., 1993; Christensen, 2001; Aurnou and Olson, 2001; Yano et al., 2003) successfully reproduce the westerly equatorial jets, but the models generate fewer jets in the middle and high latitudes. We do not address these issues. The global wind profile including strong equatorial jets will be postponed for further research.

2. Numerical method

Two-dimensional flow in a rapidly rotating fluid is governed by the QG potential vorticity equation (Pedlosky, 1987; Andrews et al., 1987):

$$\frac{\partial q}{\partial t} + J(\psi, q) = S + F, \tag{1}$$

where the potential vorticity q is $\nabla^2\psi + \beta y - \psi/L_d^2$, ψ is the streamfunction, which is proportional to the thickness of the weather layer, β is the planetary vorticity gradient, and L_d is the radius of deformation. The non-linear term is the Jacobian $J = \psi_x q_y - \psi_y q_x$. Friction F is represented by horizontal eddy diffusion: $F = \kappa_h \nabla^2 \zeta$, where the relative vorticity ζ is $\nabla^2\psi$ and κ_h is the horizontal eddy diffusion coefficient. The vorticity source S consists of two parts: (1) a positive constant S_r that represents uniform radiative cooling and (2) negative bursts, localized in space and time, that represent MC. When radiative cooling and dynamics make the thickness of the weather layer drop below a critical threshold at some place, MC will be excited there and will increase the thickness of the local weather layer. The assumption of MC excited in the regions where the thickness of the local weather layer is small implies that MC will only appear in the cyclonic bands, which are small-thickness regions in Jupiter. MC therefore creates intense regions of anticyclonic vorticity in regions where the large-scale vorticity is cyclonic, which is consistent with the observations (Little et al., 1999; Gierasch et al., 2000; Porco et al., 2003; Dyudina et al., 2004; Li et al., 2004).

We parameterize the vorticity source due to MC by a function with negative parabolic shape in lifetime and radius. The lifetime, radius and amplitude of the vorticity source due to MC are constrained by observations from Voyager, Galileo, Cassini, HST and ground-based telescopes. Large uncertainties exist in these observations, so we explore the parameter space around a standard model. Galileo and Cassini observations (Little et al., 1999; Porco et al., 2003) show that the size of MC ranges from a few hundred kilometers to a few thousand kilometers. Cassini continuum images (Li et al., 2004) suggest that the lifetime of MC is 3.5 days, but these measurements refer to storms with lifetime larger than 40 h and diameter larger than 700 km. Obviously, some small convective storms have shorter lifetime. Our standard model has lifetime of 1 day and radius of 1000 km, although we varied the lifetime between 0.3 and 6 days and the radius between 250 and 4000 km. The amplitude of the vorticity source due to MC is S_{mc}, which is given by S_r/C_{mc}, where S_r is the radiation vorticity source, and C_{mc} is the fractional area of MC over the global disk, under the

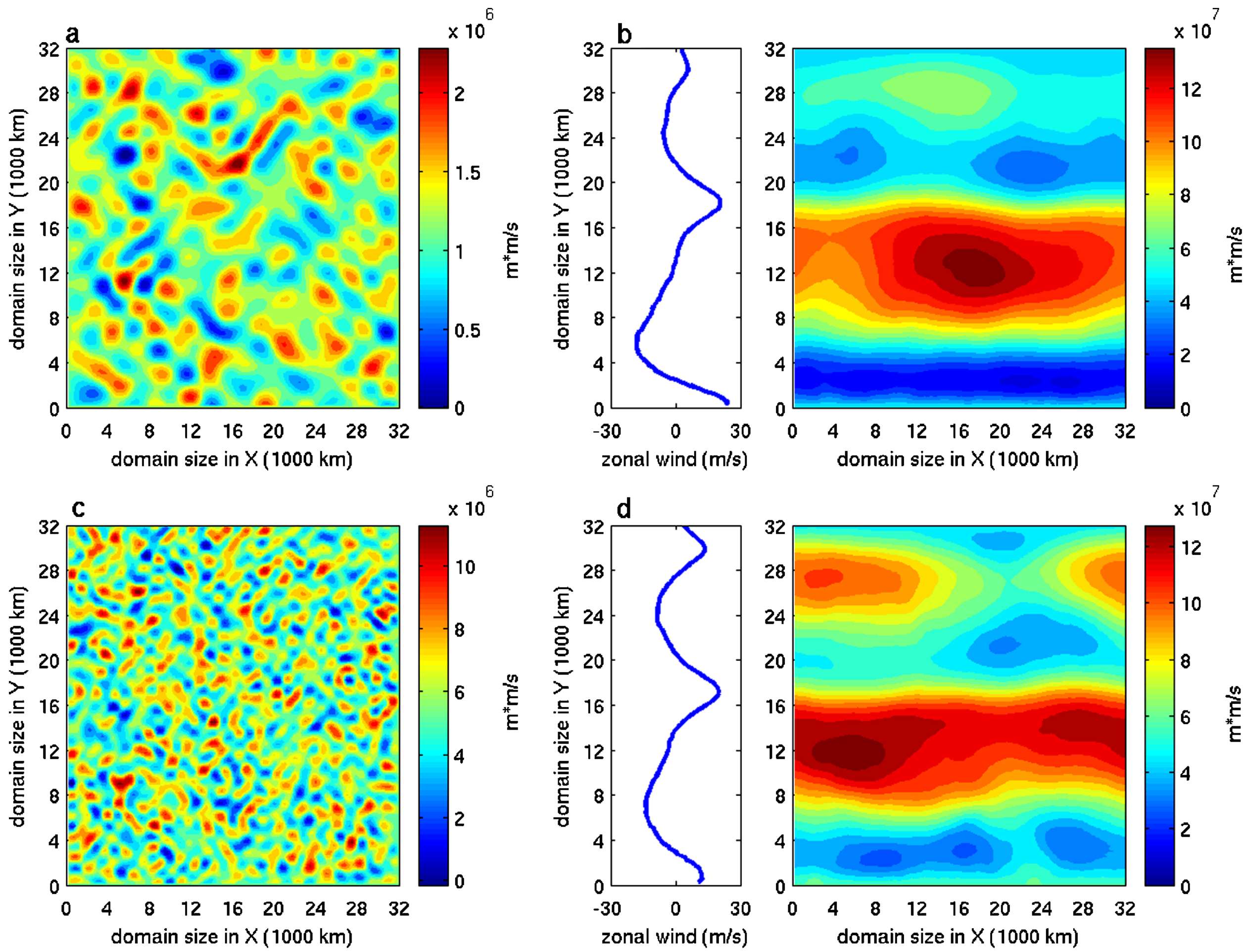

Fig. 1. Dependence of QG model on different initial random patterns: (a) and (c) are two initial random patterns with different amplitudes and length scales; (b) and (d) are the corresponding steady patterns. For these runs the parameter values are: $T_{mc} = 1$ day, $R_{mc} = 1000$ km, $S_{mc} = 1.0 \times 10^{-9}\ s^{-2}$, $L_d = 5000$ km, and $\kappa_h = 10^3\ m^2\,s^{-1}$. The domain size is 32,000 km in the x and y directions, which is equivalent to 30 longitude degrees (at latitude 30°) in the x direction and 25 latitude degrees in the y direction.

assumption that the negative vorticity source due to MC is balanced by the positive vorticity source due to uniform radiative cooling. The fractional area of MC is set to 1×10^{-4} based on the Galileo and Cassini observations (Little et al., 1999; Dyudina et al., 2004). The calculation of the radiation vorticity source S_r is given in Appendix A. We varied the amplitude of the vorticity source due to MC by a factor of 20. The horizontal eddy diffusion κ_h is set to $10^3\ m^2\,s^{-1}$ to give horizontal eddy diffusion the same net effect as vertical eddy diffusion, assuming that the vertical eddy diffusion is $\sim 10^{-1}\ m^2\,s^{-1}$ in the upper troposphere of Jupiter (Edgington et al., 1999) and the horizontal scale is 100 times the vertical scale for the jovian weather layer. The radius of deformation L_d on Jupiter is unknown but has been estimated by different studies. Ingersoll and Cuong (1981) suggested the radius of deformation is in the range of 500–5000 km. Achterberg and Ingersoll (1989) concluded that the radius of deformation is likely on the order of 1000 km by comparing their model results with the observations. Dowling and Ingersoll (1989) estimated the radius of deformation from the potential vorticity and offered a value of $L_d \sim 2000$ km. In this study, we set the standard value of L_d as 5000 km to guarantee small S_r, so that the corresponding S_{mc} can change in a relatively large range (see Eq. (A.5) in Appendix A). In addition, the numerical experiments in the next section show that our QG model is insensitive to the radius of deformation. Without loss of generality, we keep S_r and β constant in all experiments, which is equivalent to fixing the units of length and time.

Our numerical code for solving Eq. (1) is a finite-difference scheme with Arakawa's energy- and enstrophy-conserving algorithm in space (Arakawa, 1966) and the modified fourth-order Adams–Bashforth algorithm in time (Press et al., 1986). The latter is initiated by the Runge–Kutta method (Press et al., 1986). A periodic boundary condition is used in the x (zonal) direction, so a fast Fourier transform and an inverse fast Fourier transform can be performed. Channel walls are used in the y (meridional) direction (Holton, 1979, p. 252). Such boundary conditions allow the weather layer to change its total momentum. All numerical experiments begin with a random initial streamfunction pattern. The standard domain size is 32,000 km in the x and y directions in order to include multiple jets, although we have run cases with larger domains in the x and y directions. The space resolution is generally 250 km in both directions and the time step is 1000 s in order to capture MC. We

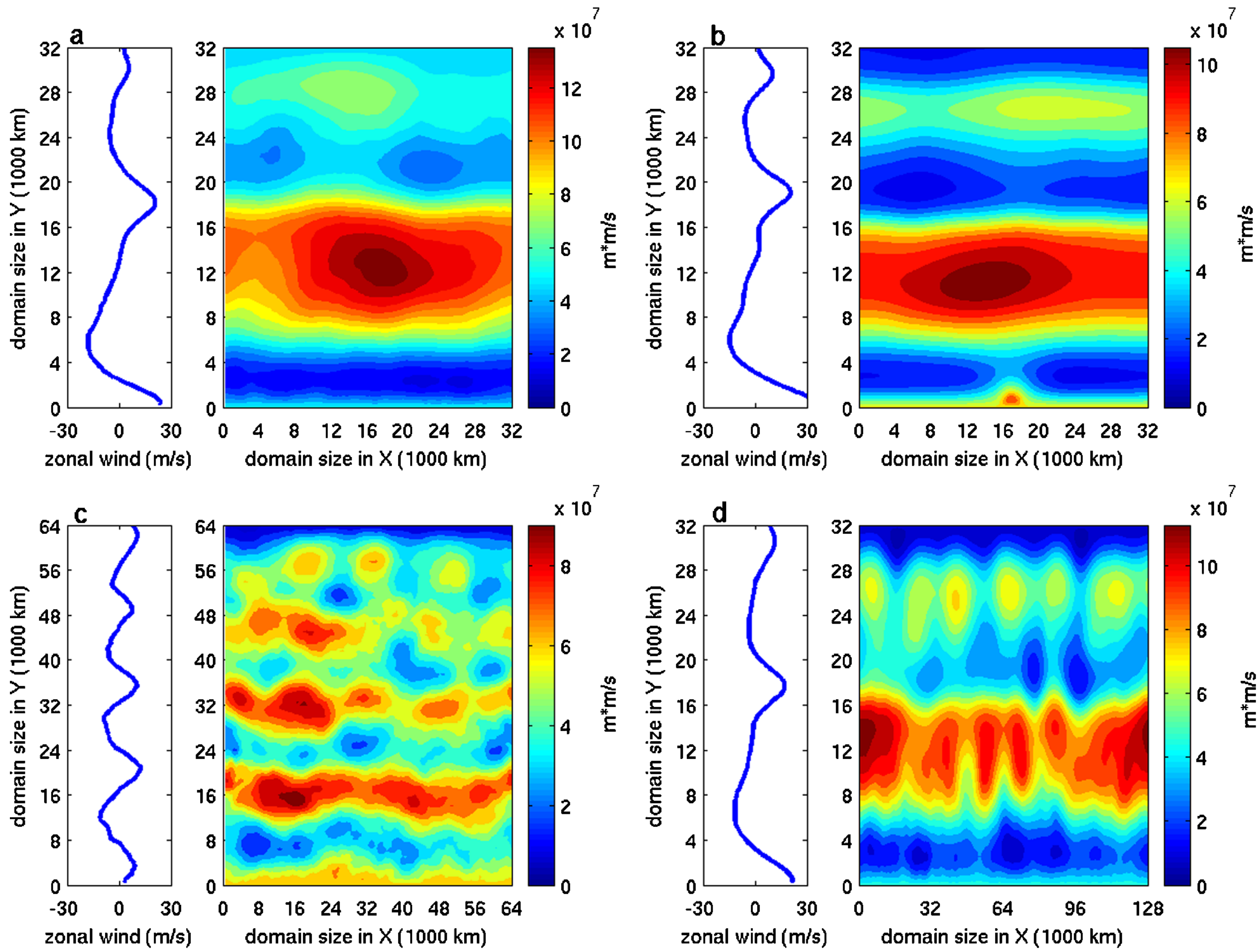

Fig. 2. Dependence of QG model on the spatial resolution and domain size. (a) Steady state of the experiment shown in Fig. 1 with space resolution 250 km and domain size 32,000 km in both directions (30 longitude degrees in the x direction and 25 latitude degrees in the y direction). (b) Steady state with space resolution 125 km and domain size 32,000 km in both directions (30 longitude degrees in the x direction and 25 latitude degrees in the y direction). (c) Steady state with space resolution 250 km and domain size 64,000 km in both directions (60 longitude degrees in the x direction and 50 latitude degrees in the y direction). (d) Steady state with space resolution 250 km and domain size 32,000 km in y direction and 128,000 km in x direction (120 longitude degrees in the x direction and 25 latitude degrees in the y direction). In all experiments of this figure, we use the same initial random pattern as in Fig. 1a and the same group of parameters as in Fig. 1.

have verified that the results are independent of the resolution, domain size, and random initial pattern. Fig. 1 displays two different initial random patterns and the corresponding steady patterns of streamfunction. The figure shows that the same steady pattern is developed from the different initial random patterns. In Fig. 2 we run the numerical model with different domain sizes by setting the same initial random pattern as in Fig. 1a and holding the same group of parameters ($T_{\mathrm{mc}} = 1$ day, $R_{\mathrm{mc}} = 1000$ km, $S_{\mathrm{mc}} = 1.0 \times 10^{-9}\ \mathrm{s}^{-2}$, $L_d = 5000$ km, and $\kappa_h = 10^3\ \mathrm{m}^2\,\mathrm{s}^{-1}$). Fig. 2 shows that the coherent zonal pattern still forms and the zonal wind profile does not change when the domain size is expanded, although some large-scale vortices are clearly displayed in the largest x domain experiment (Fig. 2d). Notice that the vortices at $\sim$26,000 km in Fig. 2d alternate in longitude (y direction) with oppositely-signed vortices at $y \sim 20{,}000$ km, which is suggestive of a Karman vortex street (Youssef and Marcus, 2003). These large-scale vortices showed in Fig. 2d are aligned around the same latitude so that they do not change the zonal wind profile. However, the coexistence of large-scale vortices and stable zonal wind is a very interesting phenomenon, which is worthy of further study. The experiments shown in Figs. 1 and 2 suggest that our numerical model is independent of the initial random pattern, the spatial resolution, and the domain size. Therefore, we use the same initial random pattern (Fig. 1a), the same spatial resolution (250 km), and the same domain size (32,000 km in the x and y directions) for all following numerical experiments.

3. Simulation results

Large uncertainties exist in the radius of deformation, the horizontal eddy diffusion, and the parameters associated with MC. A series of numerical experiments are performed to explore the parameter space. An example of these numerical experiments, which is run with standard values of parameters except for the increased amplitude of the vorticity source S_{mc}, is shown in Fig. 3. Figs. 3a–3f show a time series of stable zonal jets developing from a random initial pattern during the process of adjustment between MC and radiation. A statistically steady

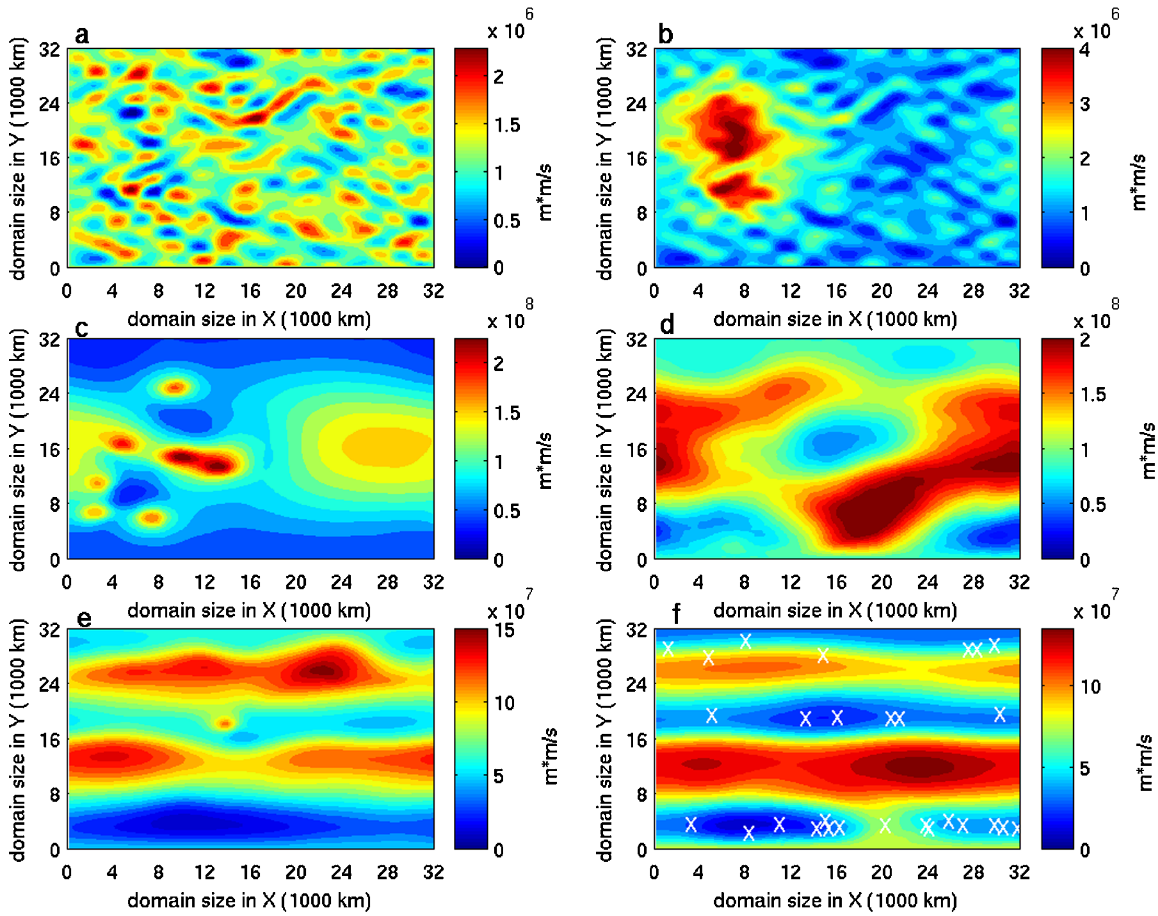

Fig. 3. Time evolution of streamfunction pattern for $T_{\mathrm{mc}} = 1$ day, $R_{\mathrm{mc}} = 1000$ km, $S_{\mathrm{mc}} = 1.1 \times 10^{-9}\ \mathrm{s}^{-2}$, $L_d = 5000$ km, and $\kappa_h = 10^3\ \mathrm{m}^2\,\mathrm{s}^{-1}$. (a) Time = 0 (initial random pattern); (b) time = 1 h; (c) time = 1 day; (d) time = 1 month; (e) time = 1 year; (f) time = 5 years. In this and all other experiments of Jupiter the values of S_r and β are $2.14 \times 10^{-14}\ \mathrm{s}^{-2}$ and $4.26 \times 10^{-12}\ \mathrm{m}^{-1}\,\mathrm{s}^{-1}$, respectively. The positions of all MCs between 1 and 5 years are shown in (f) (each bright cross 'x' represents the position of one MC). The domain size is 32,000 km in the x and y directions, which is equivalent to 30 longitude degrees in the x direction and 25 latitude degrees in the y direction.

large-scale pattern is generated after 1 year, shown in Fig. 3e. Fig. 3e also includes a MC event near the center of the domain. Fig. 3f shows the location of all MC events over a four-year period after the large-scale flow had reached a statistically steady state. This figure demonstrates that MC only appears in cyclonic bands. Fig. 4 is the corresponding zonal wind profile for the steady state phase of the experiment shown in Fig. 3. The width of the modeled stable jets (half wavelength of the zonal wind profile) is a few thousand kilometers, and the peak zonal wind is around $20\ \mathrm{m\,s^{-1}}$. Both width and strength of the modeled jets have the same order of magnitude as the observed jets outside the equatorial regions on Jupiter. Fig. 5 displays the time series of energy of the experiment shown in Fig. 3. The time series of energy suggests that the developed zonal jet pattern is in a statistically steady state after the initial adjustment.

Parameter space exploration in certain ranges around standard values is shown in Fig. 6. In general, no clear zonal patterns are developed beyond these ranges. The figure shows that the width L_{jet} and strength V_{jet} of the jets in our experiments are insensitive to the radius of deformation and the horizontal eddy diffusion coefficient. The width L_{jet} and strength V_{jet} vary directly with the parameters associated with MC: R_{mc}, T_{mc}, and S_{mc}. Hence, we define a velocity scale $V = R_{\mathrm{mc}} T_{\mathrm{mc}} S_{\mathrm{mc}}/2$ and a length scale $L = \sqrt{V/\beta}$. Fig. 7 shows that L_{jet}/L and V_{jet}/V do not change as we vary the parameters associated with MC. In other words, our experiments suggest that the width and amplitude of stable jets are controlled by the length scale L and velocity scale V. Actually, the velocity scale V represents the tangential velocity that is generated at the edge of a MC event at the end of its lifetime. The length scale L is the same as the Rhines scale $\sqrt{V_{\mathrm{jet}}/\beta}$ when the velocity scale V is proportional to the amplitude of the jets V_{jet}. The above results also suggest that the parameters of MC do not change the curvature U_{yy} of the zonal wind profile because the curvature is proportional to $V_{\mathrm{jet}}/L_{\mathrm{jet}}^2$. Further exploration of parameter space of MC verifies this point: Fig. 8 shows that the ratio between the curvature of the jets and the planetary vorticity gradient varies around 0.5, but the ratio is never larger than 1. This is consistent with the barotropic stability criterion, which says that flow is stable when $\beta - U_{yy} > 0$ and may be unstable when $\beta - U_{yy}$ changes sign.

To get the observed strong zonal wind with $\beta - U_{yy}$ changing sign around the westward jets, we invoke motions below the weather layer. The Galileo probe measured winds down to the 20-bar level and found that the equatorial eastward jet increased with depth within the weather layer and stayed constant at a high velocity from 5 to 20 bars (Atkinson et al., 1998). Study of the coupled magnetic field and zonal flow in the interior of Jupiter (Kirk and Stevenson, 1987; Liu and Stevenson, 2003) suggests that retrograde (westward) deep flow will exist in middle and high latitudes and prograde (eastward) deep flow will exist in equatorial regions. In this paper, the deep flow is assumed to be zonal and steady in the whole domain. The corresponding QG model including the zonal deep flows is dynamically equivalent to a one-layer model with meridionally varying solid bottom topography, called the reduced-gravity model

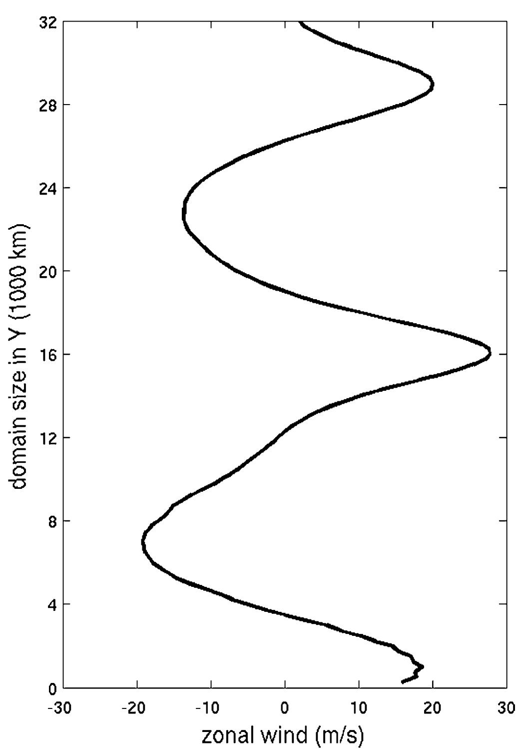

Fig. 4. Zonal wind profile for the steady state portion of the experiment shown in Fig. 3.

(Dowling and Ingersoll, 1989). The gravity g is interpreted as $g' = g\Delta\rho/\rho$, where $\Delta\rho$ is the density difference between the weather layer and the deep layer, and ρ is the mean density of the weather layer. The stability criterion for the weather layer jets is changed into (Pedlosky, 1987, pp. 478–478):

$$\beta - U_{yy} + \frac{1}{L_d^2}(U - U_2) = \beta_{\text{eff}} - U_{yy} > 0, \tag{2}$$

where the deep zonal velocity is U_2, and the effective planetary vorticity gradient is $\beta_{\text{eff}} = \beta + (U - U_2)/L_d^2$. The inequality (2) shows that the weather layer jets would be stable provided $(U - U_2) > L_d^2(U_{yy} - \beta)$. Since β_{eff} is largest when the deep flow U_2 is strong and westward relative to the weather layer flow U, the curvature U_{yy} will increase as U_2 becomes more negative. Fig. 9 shows that the observed sharp westward jets with curvature U_{yy} larger than β can be simulated with a uniform westward deep flow. The westward deep flow offers a possible and simple explanation of why the weather layer jets remain stable even though they violate the barotropic stability criterion.

The experiments for Jupiter suggest that the width and strength vary directly with the lifetime, radius, and amplitude of MC. The limited observations from Voyager, HST, ground-based telescopes, and Cassini (Sanchez-Lavega et al., 1999; Porco et al., 2005) have shown giant convective storms in Saturn's atmosphere with diameter around a few thousand kilometers and lifetime around a few weeks. In addition, observations (Beebe et al., 1992; Sanchez-Lavega et al., 1991, 1996) and numerical simulations (Sayanagi et al., 2004) suggest that very giant convective storms play an important role in the dynamics of Saturn's equatorial atmosphere. These observations also suggest that Saturn has fewer convective storms than Jupiter. We can simulate the wide and strong zonal jets of Saturn relative to Jupiter by increasing the lifetime and radius of MC and decreasing the fractional area of MC over the global disk. Fig. 10 shows a comparison between the model result and the observed zonal wind profiles in the middle latitudes of Saturn, and is to be compared with Figs. 4 and 9 for the middle latitudes of Jupiter. The result suggests that the large differences of width and strength of the jets between Jupiter and Saturn are probably due to the

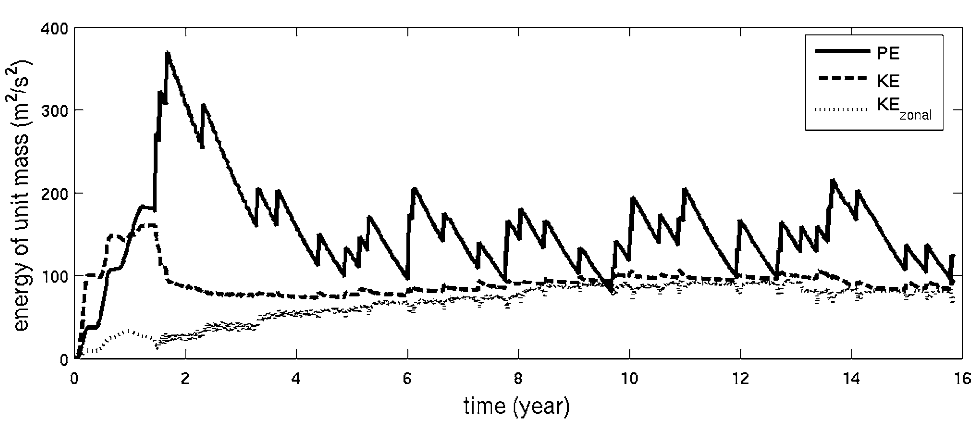

Fig. 5. Time series of global averaged energy for the experiment shown in Fig. 3: potential energy PE (solid line), total kinetic energy KE (dashed line), and zonal kinetic energy KE_{zonal} (dotted line)—the part associated with the zonal wind U. The initial energies are not zero, but they are small compared to the energies in the steady state.

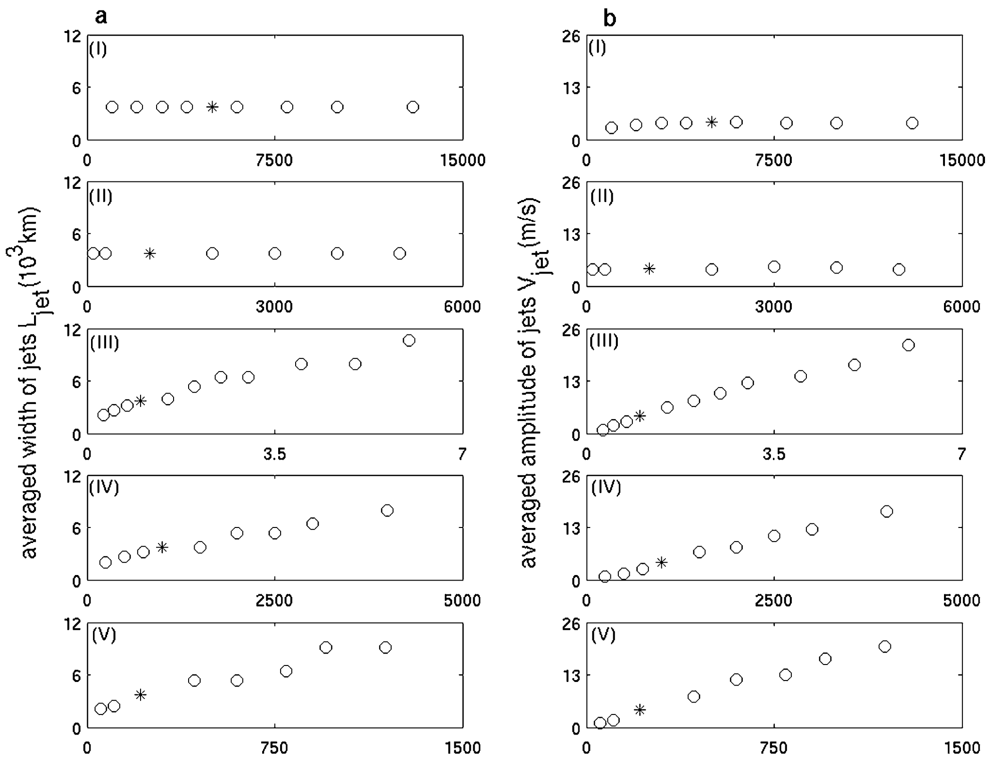

Fig. 6. Parameter space explorations. (a) Width of jets L_{jet} (half wavelength of zonal wind profile) as a function of different parameters: (I) radius of deformation L_d (unit: km); (II) horizontal eddy diffusion coefficient κ_h (unit: $\mathrm{m}^2\,\mathrm{s}^{-1}$); (III) lifetime T_{mc} of MC (unit: day); (IV) radius R_{mc} of MC (unit: km); (V) amplitude S_{mc} of vorticity source of MC (unit: $10^{-12}\ \mathrm{s}^{-2}$). (b) Same as (a) except for the amplitude of jets V_{jet}. The asterisk symbol (*) in (a) and (b) represents the experiment with the standard values ($L_d = 5000$ km, $\kappa_h = 10^3\ \mathrm{m}^2\,\mathrm{s}^{-1}$, $T_{\text{mc}} = 1$ day, $R_{\text{mc}} = 1000$ km, and $S_{\text{mc}} = 2.14 \times 10^{-10}\ \mathrm{s}^{-2}$).

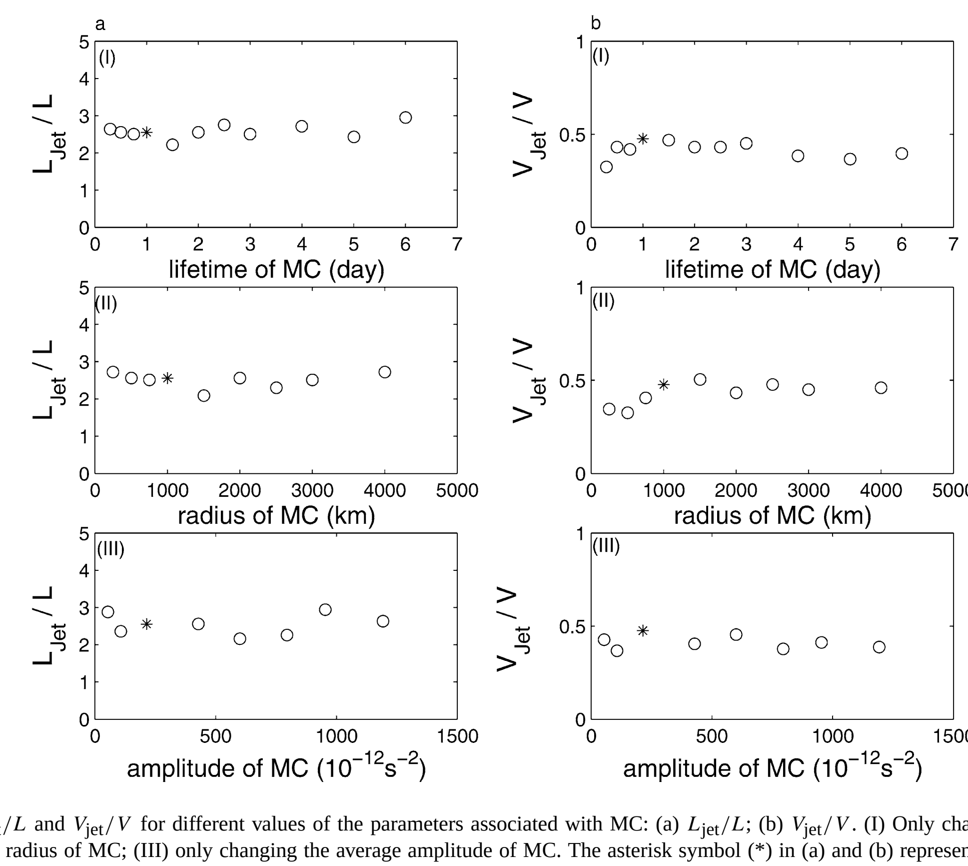

Fig. 7. The ratios L_{jet}/L and V_{jet}/V for different values of the parameters associated with MC: (a) L_{jet}/L; (b) V_{jet}/V. (I) Only changing the lifetime of MC; (II) only changing the radius of MC; (III) only changing the average amplitude of MC. The asterisk symbol (*) in (a) and (b) represents the experiment with the standard values.

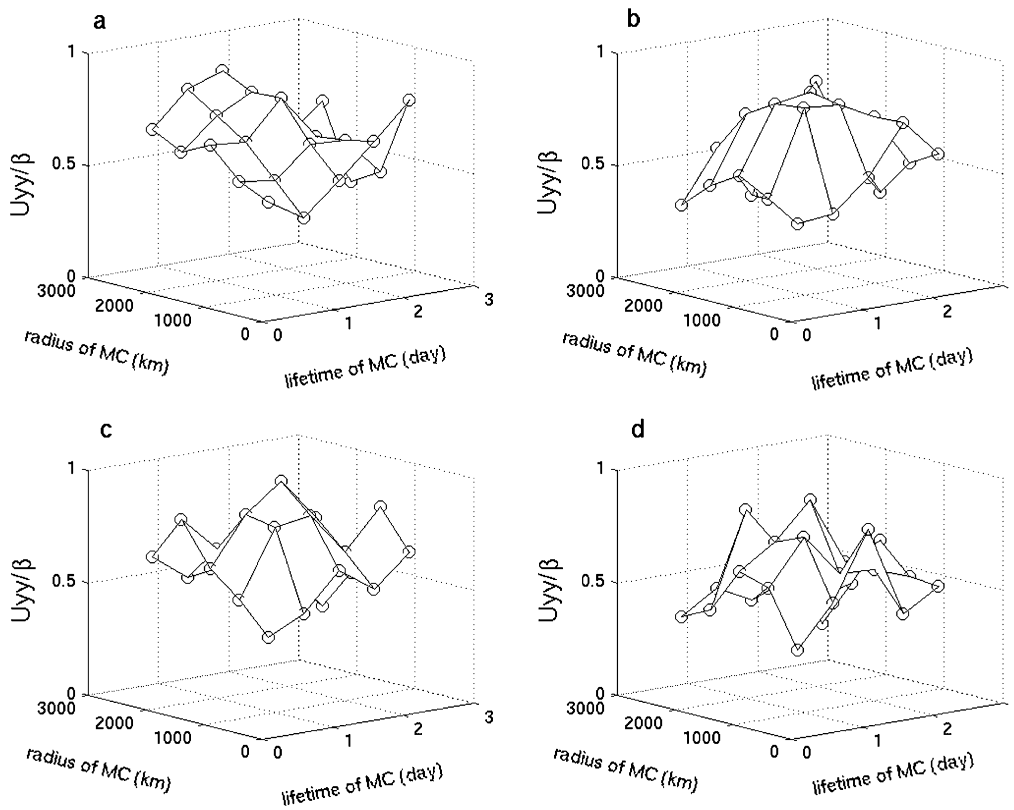

Fig. 8. Exploring the ratio U_{yy}/β in the space of lifetime and radius of MC, for four different amplitudes of MC: (a) $S_{mc} = 1.0 \times 10^{-10}\ s^{-2}$; (b) $S_{mc} = 2.0 \times 10^{-10}\ s^{-2}$; (c) $S_{mc} = 3.0 \times 10^{-10}\ s^{-2}$; (d) $S_{mc} = 4.0 \times 10^{-10}\ s^{-2}$.

different characteristics of MC (lifetime, size and frequency). What controls the characteristics of MC in Jupiter and Saturn is proposed for further study.

4. Conclusions and discussions

Our study suggests that MC can drive the zonal jets in the atmospheres of Jupiter and Saturn. The width and strength of the jets are controlled by the length scale and velocity scale associated with MC. The length scale and velocity scale also offer an explanation for the different width and strength of jets on Jupiter and Saturn. Sharp westward jets with curvature larger than the planetary vorticity gradient can be simulated with westward flow below the weather layer.

There are strong equatorial eastward jets in Jupiter and Saturn. Our QG model and previous QG models of the giant planets (Panetta, 1993; Marcus et al., 2000) are not suitable to study the equatorial regions. Decaying turbulence in a shallow water model cannot generate eastward equatorial jets (Cho and Polvani, 1996). Observations (Little et al., 1999; Sanchez-Lavega et al., 1999; Porco et al., 2003, 2005; Li et al., 2004) show that MC is active in the equatorial regions of Jupiter and Saturn. Therefore, the idea of MC driving jets should be tested in equatorial regions with new numerical models.

Laboratory models are important as a way to study atmospheric dynamics. Previous laboratory models drive the jets either with a radial temperature gradient in a rotating bowl cooled from above (Condie and Rhines, 1994) or sources and sinks of the same size on the bottom of a rotating annular tank (Sommeria et al., 1989). Here, we suggest that the latter laboratory experiment should be redone with uniform small sinks and a few large sources from the bottom.

Acknowledgments

We thank Melissa Strausberg, Glenn Flierl, and Mimi Gerstell for useful discussions and two reviewers for constructive critique. This work was supported by NASA's planetary atmospheres program.

Appendix A. Calculation of radiation vorticity source

To calculate the radiation vorticity source S_r, we start with conservation of mass for the weather layer

$$Dh/Dt + h_0 \nabla \cdot \vec{V} = \dot{h}_r + \dot{h}_{mc}, \tag{A.1}$$

where the thickness h of the weather layer is $h_0 + h'$, and the average thickness h_0 is much larger than the perturbation thickness h'. The divergence of the horizontal velocity is $\nabla \cdot \vec{V}$, the rate of thickness increase due to mass removed from the weather layer by net radiation is $\dot{h}_r$, a negative quantity, and the rate of thickness increase due to mass added to the weather layer by MC from the deep underlying layer is $\dot{h}_{mc}$, a positive quantity. The outgoing energy flux due to net radiation is assumed as F_r. Therefore, we have $F_r = -C_p \Delta\theta \rho \dot{h}_r$, where

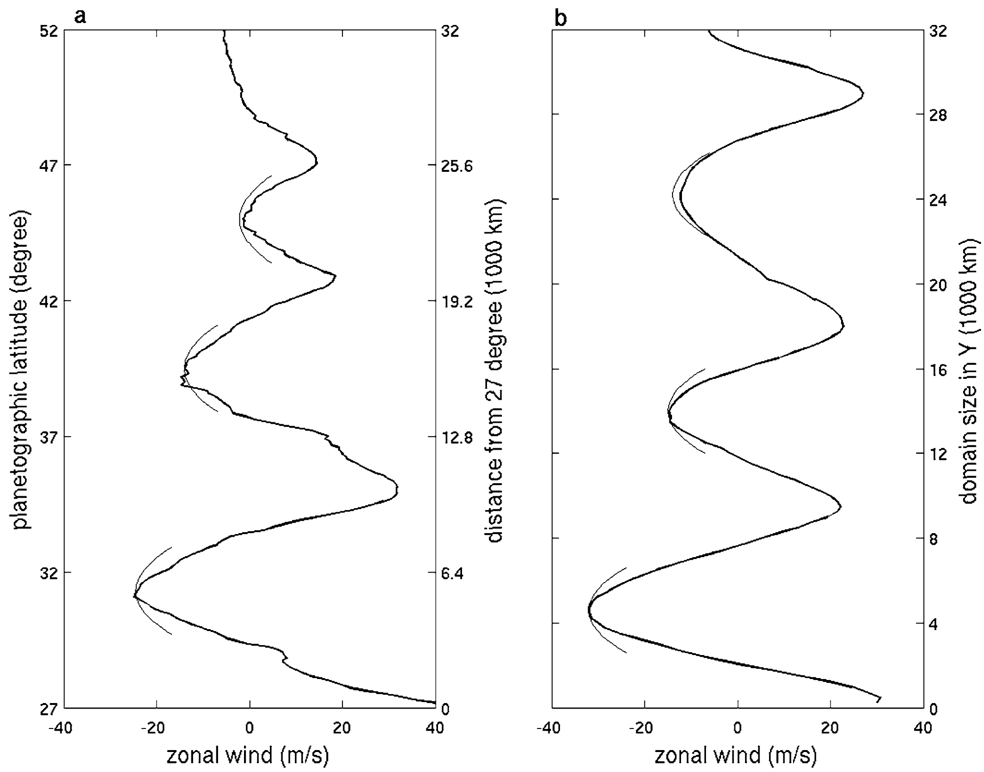

Fig. 9. Observed and simulated zonal wind profiles in the middle latitudes of Jupiter. (a) Observed wind profile in the middle latitudes of Jupiter from Cassini. The range of latitudes is chosen with the same size as the domain size of our experiments. (b) Modeled zonal wind profile of Jupiter with same parameters in Fig. 1 except for westward deep flow $U_2 = -80\ \mathrm{m\,s^{-1}}$. The thin solid curves are defined by $d^2U/dy^2 = \beta$, and are centered on the westward jet maxima.

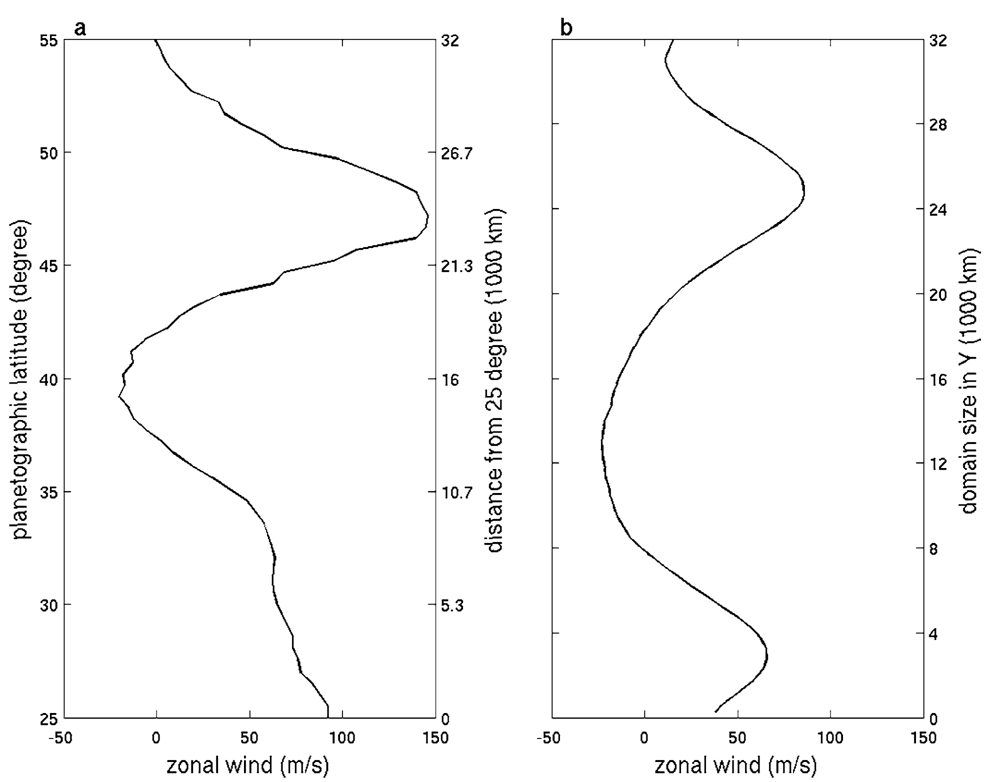

Fig. 10. Observed and simulated zonal wind profiles in the middle latitudes of Saturn. (a) Observed wind profile in the middle latitudes of Saturn from Voyager. (b) Modeled zonal wind profile of Saturn with $T_{\mathrm{mc}} = 1$ day, $R_{\mathrm{mc}} = 2000$ km, $S_r = 1.26 \times 10^{-15}\ \mathrm{s}^{-2}$, $S_{\mathrm{mc}} = 4.2 \times 10^{-11}\ \mathrm{s}^{-2}$ (fractional area $C_{\mathrm{mc}} = 3.0 \times 10^{-5}$), $L_d = 5000$ km, and $\kappa_h = 10^3\ \mathrm{m^2\,s^{-1}}$.

C_p is the specific heat, $\Delta\theta$ is the potential temperature of the weather layer minus that of the deep layer, and ρ is the mean density of the weather layer.

The large-scale vorticity equation (Holton, 1979) of the weather layer is

$$D\zeta/Dt + \beta v + f_0 \nabla\cdot \vec{V} = 0. \tag{A.2}$$

The streamfunction ψ is defined as $g'h'/f_0$, where $g' = g\Delta\rho/\rho = g\Delta\theta/\theta$ is the reduced gravity of the two-layer QG model and f_0 is the Coriolis parameter. Combining Eqs. (A.1) and (A.2) and eliminating $\nabla\cdot \vec{V}$, we have

$$D\zeta/Dt + \beta v - (f_0/h_0)(Dh/Dt - \dot{h}_r - \dot{h}_{\mathrm{mc}}) = 0. \tag{A.3}$$

From $\psi = (h'/f_0)(g\Delta\theta/\theta)$, we have $Dh/Dt = Dh'/Dt = (f_0\theta/g\Delta\theta)D\psi/Dt$. Substituting Dh/Dt into Eq. (A.3), we have

$$\begin{aligned} &D\zeta/Dt + \beta v - \left(1/L_d^2\right)D\psi/Dt = \partial q/\partial t + J(\psi, q) \\ &\quad = -(f_0/h_0)(\dot{h}_r + \dot{h}_{\mathrm{mc}}), \end{aligned} \tag{A.4}$$

where the potential vorticity q is $\nabla^2\psi + \beta y - \psi/L_d^2$ and the radius of deformation L_d is $\sqrt{gh_0\Delta\theta/(f_0^2\theta)}$. Therefore, substituting $\dot{h}_r$ into Eq. (A.4) and using the pressure $P = \rho g h_0$, we have

$$S_r = -(f_0/h_0)\dot{h}_r = \gamma g F_r/\left(P f_0 L_d^2\right), \tag{A.5}$$

where γ is the ratio of the gas constant R to the specific heat C_p. So by setting $\gamma = 1/3$, $g = 24\ \mathrm{m\,s^{-2}}$, $F_r = 5.7\ \mathrm{W\,m^{-2}}$, $P = 5\times10^5$ Pa, $f_0 = 1.7\times10^{-4}\ \mathrm{s^{-1}}$, and $L_d = 5000$ km, we have $S_r = 2.14\times10^{-14}\ \mathrm{s^{-2}}$ for Jupiter. Likewise, we have $S_r = 1.26\times10^{-15}\ \mathrm{s^{-2}}$ for Saturn by setting $\gamma = 0.28$, $g = 9\ \mathrm{m\,s^{-2}}$, $F_r = 2\ \mathrm{W\,m^{-2}}$, $P = 10\times10^5$ Pa, $f_0 = 1.6\times10^{-4}\ \mathrm{s^{-1}}$, and $L_d = 5000$ km.

References

Achterberg, R.K., Ingersoll, A.P., 1989. A normal-mode approach to jovian atmospheric dynamics. J. Atmos. Sci. 46, 2448–2462.

Andrews, D.G., Holton, J.R., Leovy, C.B., 1987. Middle Atmosphere Dynamics. Academic Press, San Diego.

Arakawa, A., 1966. Computational design for long-term numerical integration of the equations of fluid motion: Two-dimensional incompressible flow. J. Comput. Phys. 1, 119–143.

Atkinson, D.H., Pollack, J.B., Seiff, A., 1998. The Galileo Probe Doppler Wind Experiment: Measurement of the deep zonal winds on Jupiter. J. Geophys. Res. 103, 22911–22928.

Aurnou, J.M., Olson, P.L., 2001. Strong zonal winds from thermal convection in a rotating spherical shell. Geophys. Res. Lett. 28, 2557–2559.

Banfield, D., Gierasch, P.J., Bell, M., Ustinov, E., Ingersoll, A.P., Vasavada, A.R., West, R.A., Belton, M.J.S., 1998. Jupiter's cloud structure from Galileo imaging data. Icarus 135, 230–250.

Beebe, R.F., Ingersoll, A.P., Hunt, G.E., Mitchell, J.L., Muller, J.P., 1980. Measurements of wind vectors, eddy momentum transports, and energy conservations in Jupiter's atmosphere from Voyager 1 images. Geophys. Res. Lett. 7, 1–4.

Beebe, R.F., Barnet, C., Sada, P.V., Murrell, A.S., 1992. The onset and growth of the 1990 equatorial disturbances on Saturn. Icarus 95, 163–172.

Busse, F.H., 1976. A simple model of convection in the jovian atmosphere. Icarus 29, 255–260.

Carlson, B.E., Lacis, A.A., Rossow, W.B., 1992. The abundance and distribution of water vapor in the jovian troposphere as inferred from Voyager IRIS observations. Astrophys. J. 388, 648–668.

Cho, J.Y.K., Polvani, L.M., 1996. The morphogenesis of bands and zonal winds in the atmospheres on the giant outer planets. Science 273, 335–337.

Christensen, U.R., 2001. Zonal flow driven by deep convection in the major planets. Geophys. Res. Lett. 28, 2553–2556.

Condie, S.A., Rhines, P.B., 1994. A convective model for the zonal jets in the atmospheres of Jupiter and Saturn. Nature 367, 711–713.

Dowling, T.E., Ingersoll, A.P., 1989. Jupiter's Great Red Spot as a shallow water system. J. Atmos. Sci. 46, 3256–3278.

Dyudina, U.A., Del Genio, A.D., Ingersoll, A.P., Porco, C.C., West, R.A., Vasavada, A.R., Barbara, J.M., 2004. Lightning on Jupiter observed in the H_α line by the Cassini imaging science subsystem. Icarus 172, 24–36.

Edgington, S.G., Atreya, S.K., Trafton, L.M., Caldwell, J.J., Beebe, R.F., Simon, A.A., West, R.A., 1999. Ammonia and eddy mixing variations in the upper troposphere of Jupiter from HST Faint Object Spectrograph observations. Icarus 142, 342–356.

Garcia-Melendo, E., Sanchez-Lavega, A., 2001. Study of the stability of jovian zonal winds from HST images: 1995–2000. Icarus 152, 316–330.

Gierasch, P.J., Ingersoll, A.P., Banfield, D., Ewald, S.P., Helfenstein, P., Simon-Miller, A., Vasavada, A., Breneman, H.H., Senske, D.A., 2000. Observation of moist convection in Jupiter's atmosphere. Nature 403, 628–630.

Holton, J.R., 1979. Introduction to Dynamic Meteorology, second ed. Academic Press, San Diego.

Huang, H.P., Robinson, W.A., 1998. Two-dimensional turbulence and persistent zonal jets in a global barotropic model. J. Atmos. Sci. 55, 611–632.

Hueso, R., Sanchez-Lavega, A., 2001. A three-dimensional model of moist convection for the giant planets: The Jupiter case. Icarus 151, 257–274.

Hueso, R., Sanchez-Lavega, A., 2004. A three-dimensional model of moist convection for the giant planets. II. Saturn's water and ammonia moist convective storms. Icarus 172, 255–271.

Hueso, R., Sanchez-Lavega, A., Guillot, T., 2002. A model for large-scale convective storms in Jupiter. J. Geophys. Res. 107, 5075–5085.

Hunt, G.E., Godfrey, D., Muller, J.P., Barrey, R.F.T., 1982. Dynamical features in the northern hemisphere of Saturn from Voyager 1 images. Nature 297, 132–134.

Ingersoll, A.P., Cuong, P.G., 1981. Numerical model of long-lived jovian vortices. J. Atmos. Sci. 38, 2067–2076.

Ingersoll, A.P., Beebe, R.F., Mitchell, J.L., Garneau, G.W., Yagi, G.M., Muller, J.P., 1981. Interactions of eddies and mean zonal flow on Jupiter as inferred from Voyager 1 and 2 images. J. Geophys. Res. 86, 8733–9743.

Ingersoll, A.P., Beebe, R.F., Conrath, B.J., Hunt, G.E., 1984. Structure and dynamics of Saturn's atmosphere. In: Gehrels, T., Matthews, M.S. (Eds.), Saturn. Univ. of Arizona Press, Tucson, pp. 195–238.

Ingersoll, A.P., Gierasch, P.J., Banfield, D., Vasavada, A.R., 2000. Moist convection as an energy source for the large-scale motions in Jupiter's atmosphere. Nature 403, 630–632.

Kirk, R.L., Stevenson, D.J., 1987. Hydromagnetic constraints on deep zonal flow in the giant planets. Astrophys. J. 316, 836–846.

Lewis, J.S., 1969. The clouds of Jupiter and the NH_3–H_2O and NH_3–H_2S systems. Icarus 10, 365–378.

Li, L., Ingersoll, A.P., Vasavada, A.R., Porco, C.C., Del Genio, A.D., Ewald, S.P., 2004. Life cycles of spots on Jupiter from Cassini images. Icarus 172, 9–23.

Limaye, S.S., 1986. Jupiter: New estimates of the mean zonal flow at the cloud level. Icarus 65, 335–352.

Little, B., Anger, C.D., Ingersoll, A.P., Vasavada, A.R., Senske, D.A., Breneman, H.H., Borucki, W.J., 1999. Galileo images of lightning on Jupiter. Icarus 142, 306–323.

Liu, J.J., Stevenson, D.J., 2003. Constraints on the observed zonal flows from the magnetic fields in giants. Bull. Amer. Astron. Soc. 35. 1008.

Marcus, P.S., Kundu, T., Lee, C., 2000. Vortex dynamics and zonal flows. Phys. Plasmas 7, 1630–1640.

Panetta, R.L., 1993. Zonal Jets in wide baroclinically unstable regions—Persistence and scale selection. J. Atmos. Sci. 50, 2073–2106.

Pedlosky, J., 1987. Geophysical Fluid Dynamics, second ed. Springer-Verlag, New York. p. 478.

Porco, C.C., and 23 colleagues, 2003. Cassini images of Jupiter's atmosphere, satellites, and rings. Science 299, 1541–1547.

Porco, C.C., and 34 colleagues, 2005. Cassini Imaging Science: Initial results on Saturn's atmosphere. Science 307, 1243–1247.

Press, W.H., Teukolsky, S.A., Vetterling, W.T., Flannery, B.P., 1986. Numerical Recipes: The Art of Scientific Computing. Cambridge Univ. Press, Cambridge, UK.

Rhines, P.B., 1975. Waves and turbulence on a beta-plane. J. Fluid Mech. 69, 417–443.

Roos-Serote, M., Vasavada, A.R., Kamp, L., Drossart, P., Irwin, P., Nixon, C., Carlson, R.W., 2000. Proximate humid and dry regions in Jupiter's atmosphere indicate complex local meteorology. Nature 405, 158–160.

Sanchez-Lavega, A., Colas, F., Lecacheux, J., Laques, P., Miyazaki, I., Parker, D., 1991. The Great White Spot and disturbances in Saturn's equatorial atmosphere during 1990. Nature 353, 397–401.

Sanchez-Lavega, A., Lecacheux, J., Gomez, J.M., Colas, F., Laques, P., Noll, K., Gilmore, D., Miyazaki, I., Parker, D., 1996. Large-scale storms in Saturn's atmosphere during 1994. Science 271, 631–634.

Sanchez-Lavega, A., Acarreta, J.R., Hueso, R., Rojas, J.F., Lecacheux, J., Colas, F., Gomez, J.M., 1999. An overview of Saturn's equatorial storms: 1990–1997. Astrophys. Space Sci. 263, 351–354.

Sanchez-Lavega, A., Perez-Hoyos, S., Rojas, J.F., Hueso, R., French, R.G., 2003. A strong decrease in Saturn's equatorial jet at cloud level. Nature 423, 623–625.

Sayanagi, K.M., Showman, A.P., Kursinski, E.R., 2004. Effect of a large convective storm on the atmospheric dynamics of a jovian planet. Bull. Amer. Astron. Soc. 36. 1135.

Sommeria, J., Meyers, S.D., Swinney, H.L., 1989. Laboratory model of a planetary eastward jet. Nature 337, 58–61.

Stoker, C.R., 1986. Moist convection: A mechanism for producing the vertical structure of the jovian equatorial plumes. Icarus 67, 106–125.

Sun, Z.-P., Schubert, G., Glatzmaier, G.A., 1993. Banded surface flow maintained by convection in a model of the rapidly rotating giant planets. Science 260, 661–664.

Weidenschilling, S.J., Lewis, J.S., 1973. Atmospheric and cloud structures of the jovian planets. Icarus 20, 465–476.

Williams, G.P., 1978. Planetary circulation. 1. Barotropic representation of jovian and terrestrial turbulence. J. Atmos. Sci. 35, 1399–1426.

Yair, Y., Levin, Z., Tzivion, S., 1992. Water-cumulus in Jupiter's atmosphere: Numerical experiments with an axis-symmetric cloud model. Icarus 98, 72–81.

Yair, Y., Levin, Z., Tzivion, S., 1995. Microphysical processes and dynamics of a jovian thundercloud. Icarus 114, 278–299.

Yano, J.-I., Talagrand, O., Drossart, P., 2003. Origins of atmospheric zonal winds. Nature 421, 36.

Youssef, A., Marcus, P.S., 2003. The dynamics of jovian white ovals from formation to merger. Icarus 162, 74–93.